BIOCHEMISTRY
including biophysical chemistry & molecular biology
Article

*Biochemistry* **2009,** *48,* 11045–11055 11045
DOI: 10.1021/bi900946r

# Thermodynamics of Nucleotide and Inhibitor Binding to Wild-Type and Ispinesib-Resistant Forms of Human Kinesin Spindle Protein[†]

Payal R. Sheth,*[,‡] Andrea Basso,[§] José S. Duca,[∥] Charles A. Lesburg,[∥] Polina Ogas,[‡] Kimberly Gray,[§] Lissette Nale,[§] Anthony F. Mannarino,[‡] Andrew J. Prongay,[‡] and Hung V. Le*[,‡]

[‡]*Protein Science Department, Schering-Plough Research Institute, 320 Bent Street, Cambridge, Massachusetts 02141,* [§]*Tumor Biology Department and* [∥]*Drug Design Department, Schering-Plough Research Institute, 2015 Galloping Hill Road, Kenilworth, New Jersey 07033*

*Received June 4, 2009; Revised Manuscript Received October 13, 2009*

ABSTRACT: Current antimitotic cancer chemotherapy based on vinca alkaloids and taxanes target tubulin, a protein required not only for mitotic spindle formation but also for the overall structural integrity of terminally differentiated cells. Among many innovations targeting specific mitotic events, inhibition of motor enzymes including KSP (or Eg5) has been validated as a highly productive approach. Many reported KSP inhibitors bind to an induced allosteric site near the site of ATP hydrolysis, and some have been tested in clinical trials with varying degrees of success. This allosteric site was defined in detail by X-ray crystallography of inhibitor complexes, yet complementary information on binding thermodynamics is still lacking. Using two model ATP-uncompetitive inhibitors, monastrol and ispinesib, we report here the results of thermal denaturation and isothermal titration calorimetric studies. These binding studies were conducted with the wild-type KSP motor domain as well as two ispinesib mutants (D130V and A133D) identified to confer resistance to ispinesib treatment. The thermodynamic parameters obtained were placed in the context of the available structural information and corresponding models of the two ispinesib-resistant mutants. The resulting overall information formed a strong basis for future structure-based design of inhibitors of KSP and related motor enzymes.

Kinesin spindle protein (KSP or Eg5)[1] is a member of the kinesin-5 family. They are motor ATPases primarily involved in the morphogenesis of the bipolar spindle during mitosis (*1*). Members of this family share a conserved N-terminal catalytic motor domain followed by a short (12−15 amino acids) linker leading to a coiled stalk. Functionally, KSP is a bipolar hetero-tetramer composed of two polypeptides that dimerize first to form a parallel coiled coil; then the two dimers tetramerize into an antiparallel coiled coil exhibiting two motor domains each at the distal ends. The two pairs of motor domains bridge adjacent microtubules (MT) and use energy derived from ATP hydrolysis to slide the two strands relative to each other (*2*−*4*).

KSP is uniquely expressed in dividing cells, and its motor activity is known to be essential for the formation and maintenance of the bipolar spindle. Since its initial discovery in 1991 (*5*), KSP has become a key target for selective antimitotic cancer therapy, which offers improvement over older modalities employing taxanes or vinca alkaloids that bind to tubulin, a structural protein essential not only for mitosis but also for the integrity of terminally differentiated cells (*6*). The rationale for specific inhibition of KSP over other kinesins was solidified with the discovery of monastrol (*7*). Monastrol, a cell-permeable KSP inhibitor, was shown to be an antimitotic agent that caused mitotic arrest with monopolar spindles (*7*). Further mechanistic studies revealed that monastrol did not compete for ATP or microtubule binding, suggesting the existence of an allosteric inhibitor site in KSP (*8*, *9*). The KSP·ADP·monastrol complex crystal structure confirmed that monastrol was indeed an allosteric inhibitor that bound to an induced-fit pocket formed by helices α2 and α3 and loop L5, located about 12 Å away from the nucleotide site (*10*). In addition to monastrol, several inhibitors of KSP ATPase activity that bind to the induced-fit pocket have been described in the recent literature including ispinesib (*11*), 2,5-dihydro-1*H*-pyrrole-1-carboxamides (*12*), 3,5-diaryl-4,5-dihydropyrazoles (*13*, *14*), and *S*-trityl-L-cysteines (*15*). Novel chemotypes including biaryl (*16*) and thiazole (*17*) derivatives have also been reported as ATP-competitive inhibitors, presumably binding directly at the ATP site or an allosteric site in the vicinity. Detailed structural information for these chemotypes bound to KSP is still lacking.

Taking into consideration the high intracellular ATP concentration, it is not surprising that most laboratories capitalize on the design of novel compounds that bind to the induced-fit site. Among all of the reported KSP induced-fit pocket inhibitors, monastrol and ispinesib are the most well-studied. Steady-state kinetic studies showed that monastrol noncompetitively inhibited

[†]The work was funded by Schering-Plough Corp.

*Authors to whom correspondence should be addressed. P.R.S.: telephone, (617) 499-3643; fax, (617) 499-3814; e-mail, payal.sheth@spcorp.com. H.V.L.: telephone, (617) 499-3529; fax, (617) 499-3814; e-mail, hung.le@spcorp.com.

[1]Abbreviations: KSP (Eg5), kinesin spindle protein; MT, microtubules; SDS, sodium dodecyl sulfate; ATP, adenosine 5′- triphosphate; ADP, adenosine 5′-diphosphate; ATPγS, adenosine 5′-[γ-thio]triphosphate; CD, circular dichroism; TdCD, temperature-dependent circular dichroism; ITC, isothermal titration calorimetry; DMSO, dimethyl sulfoxide; HEPES, *N*-(2-hydroxyethyl)piperazine-*N*′-2-ethanesulfonic acid; PIPES, piperazine-1,4-bis(2-ethanesulfonic acid); DTT, dithiothreitol; ESI-MS, electrospray ionization mass spectrometry; LC-MS, liquid chromatography mass spectroscopy; DSC, differential scanning calorimetry; TCEP, tris(2-carboxyethyl)phosphine hydrochloride; rms, root mean square; WT, wild type.


Published on Web 10/13/2009

microtubule binding but not ATP binding in inhibition of KSP ATPase activity (*18*, *19*). Further pre-steady-state MT association kinetic studies in the presence and absence of monastrol confirmed that monastrol altered the ability of KSP to associate with MTs (*19*). Ispinesib is a quinazolinone inhibitor of KSP that is currently being tested in multiple phase II clinical trials. The steady-state and pre-steady-state kinetic studies on ispinesib showed that the mechanism of ispinesib inhibition is mostly identical to that of monastrol (*20*).

In contrast to the kinetic basis of KSP inhibition, our understanding of the thermodynamics of KSP inhibition is still rudimentary. A full understanding of KSP inhibition requires knowledge of structure as well as the thermodynamics of the ligand binding. Because the nucleotide-bound and free forms of KSP could adopt different conformations that could impact inhibitor binding, such studies must be performed with both KSP and KSP·nucleotide forms of the enzyme. Furthermore, since the KSP enzymatic ATPase cycle consists of ADP- and ATP-bound intermediates, the direct binding of the inhibitors to both KSP·ATP and KSP·ADP forms of the protein should be investigated for comparison. Here, we report a detailed study describing the thermodynamic parameters for binding interactions of KSP, nucleotides, and the two non-ATP-competitive inhibitor complexes using temperature-dependent circular dichroism (TdCD) and isothermal titration calorimetry (ITC). In the absence of microtubules, KSP has high affinity for both ADP and ATP$\gamma$S. Nucleotide binding is enthalpically favored and $Mg^{2+}$-dependent. Monastrol and ispinesib showed a strong preference for the nucleotide-bound form of KSP by TdCD and ITC. Interestingly, the inhibitors did not discriminate between the ADP- and ATP$\gamma$S-bound forms of KSP for binding in the absence of microtubules. ITC studies showed that monastrol binding was enthalpically favorable and entropically neutral. In contrast, ispinesib binding energy was due to favorable enthalpic and entropic components. The TdCD and ITC studies were also performed for the two ispinesib-resistant mutants (D130V and A133D) (*16*, *21*). Both mutants showed >1000-fold lower ispinesib binding affinity. More interestingly, the mutants, although being catalytically competent, had higher nucleotide TdCD/ITC $K_d$ and $K_{mATP}$ compared to their WT counterpart, implying some structural reorganization in the nucleotide-binding region as a consequence of the mutations in the neighboring induced-fit pocket. These results are placed in the context of the available complex structures of these ligands in the allosteric binding sites and corresponding models of the ispinesib mutants. To our knowledge, this is the first report to address the detailed thermodynamic aspects of nucleotide and inhibitor binding to KSP using ITC and TdCD techniques.

## EXPERIMENTAL PROCEDURES

Unless specifically described, all analyses were performed in the absence of microtubules.

*Materials*. Ispinesib was synthesized at Schering-Plough Research Institute. Its identity was confirmed by NMR and LC-MS. Monastrol was obtained from Calbiochem (San Diego, CA). These two KSP inhibitors were selected for study because they represent two different chemotypes and are both uncompetitive with ATP. The crystal structures of KSP·ADP in a ternary complex with monastrol or an ispinesib-like inhibitor have been reported. The nucleotides (ATP$\gamma$S and ADP) used in this study were obtained from Sigma (St. Louis, MO). The purity of the nucleotides was found to be >90% by LCMS.

*Expression and Purification of KSP Motor Domains, Wild Type and D130V and A133D Mutants*. The motor domain of KSP (amino acids 15−368) was cloned into pET24a for bacterial expression as the N-terminal hexahistidine fusion protein. Site-directed mutagenesis was performed on pET24a-KSP to generate D130V and A133D mutations. The mutations were confirmed by DNA sequencing (Genewiz Inc., S. Plainfield, NJ). The proteins were expressed in *Escherichia coli* BL21(DE3) (Novagen, San Diego, CA) cells for 4 h at 37 °C. The nucleotide-free preparations for WT and mutant forms of KSP were done as previously described (*18*) with minor modifications. Briefly, the bacterial pellet was lysed in 50 mM Tris, pH 8.0, 300 mM NaCl, 10 mM imidazole, and 1 mL/L protease inhibitor cocktail III (EMD Biosciences, San Diego, CA). After microfluidizing, the lysate was clarified by ultracentrifugation (100000*g* for 1 h at 4 °C) and loaded onto a Ni-NTA agarose column prequilibrated with lysis buffer. The protein was eluted with 0−250 mM imidazole gradient and was further purified with an S75 gel-filtration column (GE Healthcare, Piscataway, NJ). Fractions which were >95% pure based on SDS−PAGE analyses were pooled. The purified (nucleotide-free) wild-type KSP was shown to be fully active in the ATPase assay. The concentrations of WT and mutant KSP were determined in 6 M GdnHCl using UV spectrophotometry and an extinction coefficient at 280 nm of 21200 $M^{-1}$ $cm^{-1}$ based on the amino acid sequence.

*Mass Spectrometry*. The molecular weights of wild-type and mutant KSP proteins were determined by ESI-ion-trap-MS performed on an LTQ-XL mass spectrometer through Xcalibur (Thermo-Fisher Scientific, Waltham, MA). Spectra were collected in the positive ion mode with the capillary voltage set at 88 V, the spray cone voltage at 5 kV, and the tube lens voltage at 140 V. The source temperature was set at 275 °C. The desolvation gas flow rate was kept at 10 L/h. Deconvolution of $m/z$ spectra, to mass spectra, was performed with the Promass software program (Thermo-Fisher Scientific, Waltham, MA). Chromatography was performed with an ACCELA HPLC system (Thermo-Fisher Scientific, Waltham, MA) that was interfaced to the ion-trap mass spectrometer. Reversed-phase chromatography was performed at a flow rate of 50 $\mu$L/min utilizing a C4 column, 5 $\mu$m, 50 × 0.5 mm (Higgins Analytical, Mountain View, CA) and gradient elution (0.1%−90% acetonitrile with 0.1% TFA).

*ATPase Assay*. KSP biochemical enzyme assays were performed in 384-well plates. For the assay, microtubules were stored at −80 °C and thawed at room temperature, ATP and enzyme were stored at −20 °C and thawed on ice, buffer was stored at 4 °C, and paclitaxel was stored at room temperature. Compounds were diluted in 100% DMSO to their final concentrations. Ten microgram microtubules (Cytoskeleton, Denver, CO) were reconstituted in 10 mL of tubulin buffer (80 mM PIPES, pH 6.9, 1 mM EGTA, 1 mM $MgCl_2$) plus 100 $\mu$L of 2 mM paclitaxel (Cytoskeleton, Denver, CO). Each reaction consisted of KSP motor domain (amino acids 15−368): 10 nM for WT and A133D and 25 nM for D130V. The reaction consisted of 20 $\mu$M paclitaxel (Cytoskeleton), 10 $\mu$M microtubules, 100 $\mu$M ATP (Roche, Indianapolis, IN), and kinesin buffer (20 mM ACES, pH 7.0, 1 mM EGTA, 1 mM $MgCl_2$, 25 mM KCl, 1 mM DTT). The 10 $\mu$M microtubule concentration was measured to be >50-fold above the $K_{1/2MT}$ for all three proteins (Table 1). For each reaction, 19 $\mu$L containing KSP motor domain, paclitaxel, microtubules, and kinesin buffer was combined with 1 $\mu$L of compound. The reaction was started by the addition of 5 $\mu$L of ATP and was allowed to run for 1 h at

Table 1: Kinetic Data for WT and Ispesinib-Resistant Mutant Forms of KSP[a]

| enzyme | $K_{mATP}$ ($\mu$M) | $k_{cat}$ ($s^{-1}$) | $k_{cat}/K_m$ ($\mu M^{-1}$ $s^{-1}$) | $K_{1/2MT}$ ($\mu$M) | $IC50_{ispinesib}$ ($\mu$M) | $IC50_{monastrol}$ ($\mu$M) |
|---|---|---|---|---|---|---|
| WT | 38 ± 3.1 | 14 ± 0.15 | 0.36 ± 0.03 | 0.2 ± 0.04 | 0.005 ± 0.0005 | 50 ± 2 |
| D130V | 70 ± 2.5 | 7 ± 0.2 | 0.10 ± 0.02 | 0.15 ± 0.06 | > 3 | > 100 |
| A133D | 55 ± 1.5 | 10 ± 0.06 | 0.18 ± 0.01 | 0.2 ± 0.03 | 1.4 ± 0.02 | > 100 |

[a]MT-stimulated ATPase activities of WT and mutant forms of the protein were analyzed as described in Experimental Procedures. The M−M kinetic parameter values reported represent ± the standard error for unweighted nonlinear least-squares regression analyses of the enzymatic data. The IC50 values reported represent ± the standard error from three independent experiments.

room temperature. The reaction was stopped by adding 50 $\mu$L of Biomol Green (Biomol International, Plymouth Meeting, PA). After an additional 30 min, absorbance at 620 nm was measured using an Envision plate reader (Perkin-Elmer, Waltham, MA). For kinetic analyses, the $OD_{620}$ values were plotted as a function of time for each reaction to calculate the slope of the reaction. The slope was converted to velocity, $V_o$ (nmol $min^{-1}$), using a standard curve that converted the $OD_{620}$ values to nanomoles of phosphate. Estimations of $K_m$, $V_{max}$, and $k_{cat}$ for KSP proteins were derived by fitting the velocity data at different ATP concentrations to the Michaelis−Menten (M−M) equation. The experimental data for wild-type KSP and the mutants fit the M−M equation with a goodness of fit $R^2$ of > 0.97. For IC50 determinations, dose−response curves were plotted from inhibition data generated each in duplicate, from 8 point serial dilutions of inhibitory compounds. Concentration of compound was plotted against enzyme activity (OD reading). To generate IC50 values, the dose−response curves were then fit to a standard sigmoidal curve, and IC50 values were derived by nonlinear regression analysis.

*Circular Dichroism (CD) and Temperature-Dependent Circular Dichroism (TdCD).* The CD experiments were performed on a Jasco J810 spectropolarimeter equipped with a six-cell piezoelectric temperature controller (Jasco Inc., Easton, MD). The far-UV CD spectra were recorded between 200 and 250 nm for all KSP proteins using a 1 nm slit width and 1 mm path-length cell thermostated at 25 °C. The wavelength scan rate was maintained at 50 nm/min. The cell contained 10−12 $\mu$M KSP dissolved in 20 mM PIPES, pH 6.8, 300 mM NaCl, and 1 mM DTT, thoroughly degassed prior to the experiment. All of the proteins were dialyzed into the assay buffer prior to the experiments, and the dialysate was subsequently used as blank for subtraction from the respective protein spectra and the latter was converted into mean molar ellipticity. The secondary structure parameters of the WT and the mutants were estimated with the Jasco secondary structure manager software using the reference CD data set-Yang.jwr (*22*).

For the thermal denaturation studies, ellipticity was monitored at 230 nm as a function of temperature with a 1 mm path-length cell. The thermal scan rate was 0.5 °C/min with a 4 s response time and 30 s equilibration between measurements. Stock protein was diluted to 8−10 $\mu$M with 20 mM PIPES, pH 6.8, 300 mM NaCl, and 1 mM DTT. Nucleotides were tested at 0.5 mM concentration, and the compounds (monastrol and ispinesib) were tested at 50−75 $\mu$M in the presence or absence of 0.25−0.5 mM nucleotide concentrations as indicated in individual experiments. The final DMSO concentration was 1% for the TdCD experiments with compounds present. Data were analyzed using the Jasco software to calculate protein melting temperatures ($T_m$) and the enthalpy of unfolding $\Delta H_u$. The protein melting temperatures were reported as the average from two or three separate experiments.

The relationship between ligand binding and protein stability as detected by changes in the midpoint of unfolding ($T_m$) has been well documented (*23*, *24*), and $K_d$ values can be estimated from the $\Delta T_m$ determined by temperature-dependent circular dichroism (TdCD) (*25*). Equation 1 (*25*) was used to calculate $K_d$ values for ispinesib and monastrol binding to WT and mutant forms of KSP. The ligand binding constant ($K_L(T)$) can be calculated at any temperature ($T$) by the equation:

$$K_L(T) = K_L(T_m)\exp\left\{\left(\frac{-\Delta H_L(T)}{R}\right)\left(\frac{1}{T}-\frac{1}{T_m}\right) + \left(\frac{\Delta C_{pL}}{R}\right)\left[\ln\frac{T}{T_m}+1-\frac{T}{T_m}\right]\right\} \quad (1)$$

where $T_m$ is the midpoint of unfolding in the presence of ligand, $\Delta H_L$ is the enthalpy of binding, $\Delta C_{pL}$ is the ligand binding heat capacity, and $K_L(T_m)$ is the ligand binding constant at $T_m$. If estimates for both $\Delta H_L$ and $\Delta C_{pL}$ are available, then the ligand binding constant, $K_L(T)$, can be calculated at any temperature $T$ (assuming that the heat capacity term is temperature independent). $K_L(T_m)$ can be calculated by the equation:

$$K_L(T_m) = \{\exp\{-(\Delta H_u(T_0)/R)(1/T_m - 1/T_0) + (\Delta C_{pu}/R)[\ln(T_m/T_0)+(T_0/T_m)-1]\} - 1\}/[L_{T_m}] \quad (2)$$

where $T_0$ is the midpoint of unfolding for the unliganded protein, $T_m$ is the midpoint of unfolding in the presence of ligand, $\Delta H_u$ is the enthalpy of protein unfolding, $\Delta C_{pu}$ is the heat capacity associated with protein unfolding, and $[L_{T_m}]$ is the free concentration of ligand at $T_m$. Unless otherwise specified, $\Delta H_L$ values were used from the ITC experimental data or assumed to be −7 kcal/mol, where data were unavailable, and $\Delta C_{pL}$ was set to zero for TdCD-determined $K_L(T)$.

In nonideal systems, the loss of secondary structure in TdCD as a function of temperature is due to both structural unfolding and irreversible protein aggregation. Large proteins such as KSP tend to exhibit aggregation at high temperatures at the high protein concentrations required for TdCD experiments. As a result, the observed unfolding profile is a reflection of structural unfolding as well as aggregation. However, previous studies have suggested aggregation to be a slower process compared to the relatively faster native-to-unfolded reaction (*26*). Therefore, in application to KSP unfolding, we assume the aggregation step is much slower than the native-to-unfolded reaction.

*Isothermal Titration Calorimetry.* Purified proteins were dialyzed extensively against 20 mM PIPES at pH 6.8, 300 mM NaCl, and 2 mM BME. The protein was diluted to the appropriate concentration (either 10−30 $\mu$M) with dialysate buffer immediately prior to the experiment. Protein concentrations were measured in 6.7 M guanidine hydrochloride buffered with 20 mM phosphate at pH 7.0 at 280 nM using an extinction coefficient

of 21200 $M^{-1}$ $cm^{-1}$. Nucleotide solutions of ADP and ATP$\gamma$S were prepared in the dialysis buffer immediately prior to each titration. Nucleotide concentrations were measured using an extinction coefficient of 15400 $M^{-1}$ $cm^{-1}$ at 260 nm for adenosine. Compounds were prepared in 100% DMSO and added such that the final solution contained less than or equal to 1% DMSO. For these titrations, DMSO was added to the protein solution to the same percentage. Monastrol was used at 200 $\mu$M concentration, and ispinesib was used at 250 $\mu$M in all experiments. Both compounds were shown to be soluble at these concentrations under the ITC solution conditions by nephelometry using a Nepheloskan Ascent 100 nephelometer (Labsystems). For direct nucleotide (ADP/ATP$\gamma$S) binding experiments, 300 $\mu$M nucleotide + 5 mM $MgCl_2$ was injected into 30 $\mu$M protein (WT or mutants) + 5 mM $MgCl_2$; for direct monastrol/ispinesib binding to the WT KSP·nucleotide complex, 200−250 $\mu$M compound with 500 $\mu$M nucleotide (ADP/ATP$\gamma$S) + 5 mM $MgCl_2$ was injected into 10−20 $\mu$M KSP supplemented with 500 $\mu$M nucleotide (ADP/ATP$\gamma$S) + 5 mM $MgCl_2$. The direct binding of monastrol/ispinesib to mutant forms of the protein gave a poor signal, which could not be increased because of compound solubility limitations at higher concentrations. In the reverse titration (protein in syringe), KSP performed aberrantly and seemed to denature at low concentrations while stirring.

ITC experiments were performed with a Microcal $ITC_{200}$ titration calorimeter (Microcal Inc., North Hampton, MA). Protein and nucleotide solutions were centrifuged for 5−10 min at room temperature prior to loading the samples in the ITC cell and syringe. All titrations were carried out at 20 °C with a stirring speed of 350 rpm and a 180 s duration between each 3 $\mu$L injection. Parallel experiments were performed by injecting the nucleotide into the buffer or the buffer into the protein to determine heats of dilution. The heats of dilution were negligible in all cases and were subtracted from their respective titrations prior to data analysis.

Thermodynamic parameters $N$ (stoichiometry), $K_a$ (association constant), and $\Delta H$ (enthalpy change) were obtained by nonlinear least-squares fitting of experimental data using a single-site-binding model of the Origin software package (version 5.0) provided with the instrument. The free energy of binding ($\Delta G$) and entropy change ($\Delta S$) were obtained using the equations:

$$\Delta G = -RT \ln K_a \quad (3)$$

$$\Delta G = \Delta H - T\Delta S \quad (4)$$

The affinity of the nucleotide to protein and protein/inhibitor complex is given as the dissociation constant ($K_d = 1/K_a$). For each protein·nucleotide·compound interaction, two or three titrations were performed. Titration data were analyzed independently, and the thermodynamic values obtained were averaged.

*Molecular Modeling*. The crystal structure of KSP in complex with ADP/$Mg^{2+}$ and *N*-(3-aminopropyl)-*N*-((3-benzyl-5-chloro-4-oxo-3,4-dihydropyrrolo[2,1-*f*][1,2,4]triazin-2-yl)-(cyclopropyl)methyl)-4-methylbenzamide (PDB access code: 2gm1) was utilized as the frame of reference (*27*). All water molecules were deleted, and hydrogen atoms were added using Maestro 7.0 (*28*). Hydrogen atoms were minimized with all heavy atoms fixed (Macromodel (*28*) v9.0, MMFF94s force field, GB/SA implicit solvation model, PRCG, convergence threshold 0.05). After deleting the ligand, a Glide (*29*, *30*) grid was computed for the KSP·ADP/$Mg^{2+}$ ternary complex (Impact v3.5) (*28*) with an inner box region (the ligand midpoint remains within this box during docking) of 10 Å and an outer box region of 24 Å. The grid midpoint was defined by the centroid of one of the ligands in the data set. Ispinesib was docked using the program Glide extra precision (XP, Impact v4.0217) with default settings (Maestro v7.0).

## RESULTS

*Purification and Characterization of Wild-Type and Ispinesib-Resistant Forms of KSP*. The construct used for our studies contained amino acids 15−368 of the KSP protein corresponding to the core motor domain and a portion of the neck linker. The construct, therefore, retained all of the structural elements required for ATP hydrolysis. The expression of the N-terminal hexahistidine-tagged version of the construct for WT, D130V, and A133D in *E. coli* was accomplished as described under Experimental Procedures. All three proteins were isolated from the soluble fraction of the cell lysate and were purified to >95% homogeneity as evaluated by SDS−PAGE (see Supporting Information, Figure S1) and densitometric scanning of the relevant Coomassie Blue stained band. Purified WT, A133D, and D130V KSP proteins had the expected masses and amino acid sequences based on mass spectrometry and N-terminal sequencing results (data not shown). Enzymatic characterization showed that the three forms of KSP were capable of catalysis (detailed enzymatic characterization below). All three proteins were subjected to size-exclusion chromatography to determine their oligomerization state. The three KSP forms eluted at a volume corresponding to an apparent molecular mass consistent with a monomeric form of the protein (Supporting Information, Figure S2). No KSP protein was apparent in the fractions corresponding to the void volume of the Superdex 75 26/60 gel-filtration column, confirming the homogeneity of the protein preparation with no significant aggregation.

*Steady-State Kinetic Analysis of Human KSP ATPase Activity and Inhibition by Ispinesib and Monastrol*. All KSP constructs exhibited ATPase activities as detected by a phosphate hydrolysis assay (BioMol Green). Under steady-state conditions and in the presence of microtubules (MT), the $K_{mATP}$ and $k_{cat}$ for WT KSP was 38 ± 3.1 $\mu$M and 14 ± 0.15 $s^{-1}$, respectively, resulting in a catalytic efficiency of $k_{cat}/K_m = 0.36 \pm 0.03$ $\mu M^{-1}$ $s^{-1}$ (Table 1) consistent with previously reported values (*11*, *31*). Close analysis of the kinetic parameters revealed small but significant differences in the $K_{mATP}$ and $k_{cat}$ ($p < 0.001$) between WT KSP and its mutant counterparts (A133D $K_{mATP} = 55 \pm 1.5$ $\mu$M, $k_{cat} = 10 \pm 0.06$ $s^{-1}$ and D130V $K_{mATP} = 70 \pm 2.5$ $\mu$M, $k_{cat} = 7 \pm 0.2$ $s^{-1}$) (Table 1). D130V had lower catalytic efficiency ($k_{cat}/K_m = 0.10 \pm 0.02$ $\mu M^{-1}$ $s^{-1}$) compared to A133D ($k_{cat}/K_m = 0.18 \pm 0.01$ $\mu M^{-1}$ $s^{-1}$). The order of catalytic efficiency among the three species is therefore WT > A133D > D130V. No significant difference in the $K_{1/2MT}$ values of three KSP proteins was observed in the enzymatic assay (Table 1).

As expected, concentration−response studies of ispinesib inhibition of KSP proteins revealed that it was a potent inhibitor of the MT-stimulated ATPase activity (Table 1) of WT KSP with $IC50_{ispinesib} = 5 \pm 0.5$ nM, consistent with the previous report on the discovery of the compound (*11*). The inhibition by ispinesib in the mutant forms of KSP was severely compromised with $IC50_{ispinesib}$ values of >3 $\mu$M and 1.4 ± 0.02 $\mu$M for D130V and A133D mutants, respectively (Table 1). Monastrol, which

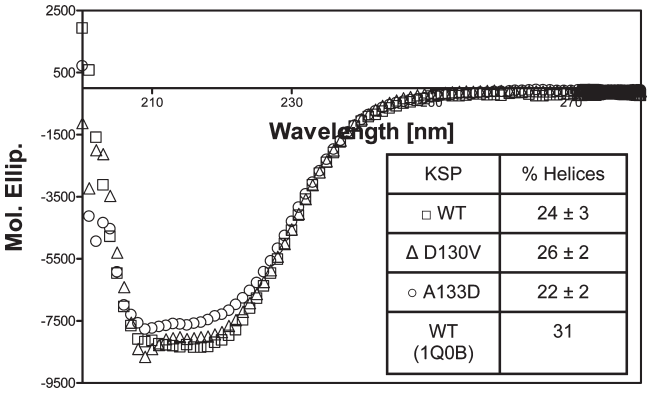


FIGURE 1: Far-UV CD spectra of WT and mutant KSP. Circular dichroism spectra for WT (□), A133D (○), and D130V (△) forms of KSP in 20 mM PIPES, pH 7.5, 300 mM NaCl, and 1 mM DTT buffer at 20 °C. The protein concentrations were 10−12 $\mu$M. Helical content was determined using the secondary structure prediction software by Jasco (inset). The % helical content is an average of three different experimental scans analyzed separately for secondary structure calculations.

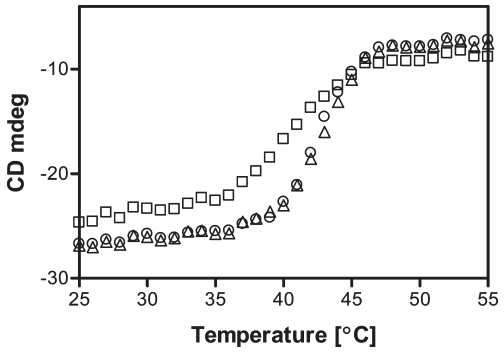


FIGURE 2: TdCD analyses of nucleotide binding to WT KSP. CD thermal denaturation curves for WT KSP (□), WT KSP + ADP (○), and WT KSP + ATP$\gamma$S (△). Ellipticity (mdeg) was measured at 230 nm as a function of temperature (22−75 °C). Protein concentrations were 10−12 $\mu$M, ADP concentration was saturating at 0.5 mM, and ATP$\gamma$S concentration was 0.5 mM in 20 mM PIPES, pH 7.5, 300 mM NaCl, 5 mM $MgCl_2$, and 1 mM DTT. The temperature was increased at 1 °C/min in a 1 mm path-length quartz cuvette.

binds in the same allosteric site as ispinesib, showed similar effect on the ATPase activity of the KSP proteins as ispinesib. Monastrol inhibited WT KSP protein ATPase activity in the micromolar range ($IC50_{monastrol}$ of 50 ± 2 $\mu$M) while no significant inhibition ($IC50_{monastrol}$ > 100 $\mu$M) could be demonstrated for the D130V and A133D mutants (Table 1). These results confirm and extend the previous report (*16*, *21*) indicating that these two mutations confer resistance to the inhibitory effect of ispinesib. The order of resistance, D130V > A133D, follows the same trend as the effect of ATPase catalytic efficiency.

*Circular Dichroism Studies of WT KSP and Mutants*. The far-UV spectra for all three KSP species, WT and A133D and D130V mutants, were collected to confirm the folding and structural integrity of the three purified proteins (Figure 1). The helical character of the proteins is apparent on the basis of the double minimum at 222 and 209 nm, although the maximum at 193 nm could not be observed due to buffer interference and high noise. Secondary structure prediction according to the method of Yang et al. (*22*) resulted in a calculated helical content of 24 ± 3%, 26 ± 2%, and 22 ± 2% for WT and D130V and A133D mutants, respectively. The secondary structure of our WT KSP enzyme is slightly lower (24 ± 3% versus 31%) than the crystal structure of the KSP·ADP complex described in the current literature (*32*). However, the differences between the WT and mutant forms of the enzyme were not statistically significant. Based on these results, the two point mutations, D130V and A133D, did not cause significant changes in the overall secondary structure of the KSP motor domain. The significant negative ellipticity observed in the 225−230 nm range rendered a suitable probe for monitoring the unfolding of the three KSP proteins using TdCD.

*TdCD of WT KSP: Effects of Nucleotides, Magnesium, and Inhibitors*. Using TdCD, we first investigated the binding of nucleotides to the wild-type KSP form. In the absence of microtubules, KSP showed a clear stabilizing shift in $T_m$ relative to the apoprotein of approximately 2.4 ± 0.14 °C $\Delta T_m$ in the presence of 0.5 mM ATP$\gamma$S, corresponding to a calculated (using $\Delta H_L$ from ITC data, Table 4) $K_d$ of 3 $\mu$M (Figure 2, Table 2). The $\Delta T_m$ for ADP, under identical experimental conditions, was similar to ATP$\gamma$S (Figure 2, Table 2). Although magnesium was observed in the KSP·monastrol·ADP crystal structure (*10*), the relative contribution of $Mg^{2+}$ in the docking of the nucleotides to KSP was unknown. To address this issue, we examined the effects of $Mg^{2+}$ on the interaction of KSP with ADP using TdCD. No detectable nucleotide binding ($\Delta T_m$ < 0.5 °C) was observed in the absence of $Mg^{2+}$ by TdCD (Table 2). The $Mg^{2+}$ dependence was also seen for ATP$\gamma$S binding (data not shown). Thus, $Mg^{2+}$ is required for nucleotide binding to KSP and was, therefore, included in the subsequent experiments. These nucleotide TdCD binding studies indicate the following: (1) the relative affinities for ATP$\gamma$S and ADP for apo KSP were similar; (2) $Mg^{2+}$ is required for binding of nucleotides.

In the presence of 50 $\mu$M ispinesib, the KSP·ADP complex showed a large 12.5 ± 0.3 °C shift in $\Delta T_m$ corresponding to single-digit nanomolar affinity (Figure 3, Table 3). Interestingly, these results are consistent with the reported $K_i$ values for ispinesib measured in the presence of microtubules (*11*) and also consistent with the IC50 value determined in Table 1. Additional studies using the KSP·ATP$\gamma$S complex instead of KSP·ADP showed similar $\Delta T_m$ in the presence of 50 $\mu$M ispinesib (data not shown). The apo KSP form in buffer containing 5 mM $MgCl_2$

Table 2: TdCD Analyses of WT KSP[a]

| preloaded mix (WT KSP + 5 mM $MgCl_2$) | $T_m$ (°C) | $\Delta T_m$ (°C) | TdCD $K_d$[b] ($\mu$M) |
|---|---|---|---|
| +DMSO | 40.7 ± 0.07 | | |
| +DMSO + 0.5 mM ATP$\gamma$S | 43.1 ± 0.07 | 2.4 ± 0.14 | 3 |
| +DMSO + 0.5 mM ADP | 42.9 ± 0.07 | 2.2 ± 0.14 | 0.7 |
| +50 $\mu$M ispinesib | 43.7 ± 0.04 | 3 ± 0.1 | 2.3 |
| +75 $\mu$M monastrol | 40.7 ± 0.07 | < 0.5 | > 30 |
| **preloaded mix (WT KSP, no $MgCl_2$)** | **$T_m$ (°C)** | **$\Delta T_m$ (°C)** | **TdCD $K_d$[b] ($\mu$M)** |
| +DMSO | 40.7 ± 0.07 | | |
| +DMSO + 0.5 mM ADP | 40.2 ± 0.14 | −0.5 ± 0.2 | |
| +DMSO + 0.5 mM ADP + 50 $\mu$M ispinesib | 50.1 ± 0.14 | 9.4 ± 0.2 | 0.015 |

[a]TdCD analyses were performed and analyzed as described in the Experimental Procedures under conditions shown in the preloaded mix column. [b]Assuming $\Delta H_L$ for ADP = −40 kcal/mol, $\Delta H_L$ for ATP$\gamma$S = −25 kcal/mol, and $\Delta H_L$ for monastrol = −8 kcal/mol, $\Delta T_m$ = $T_m$ (+ligand) − $T_m$ (apo protein) using 50−75 $\mu$M compound or 0.5 mM nucleotide. Standard error values are from two to three experiments.

showed a 3 ± 0.1 °C $\Delta T_m$ (TdCD $K_d$ at 20 °C ~2 $\mu$M) in the presence of 50 $\mu$M ispinesib (Table 2). These TdCD results demonstrated that the apo KSP protein, in the absence of nucleotides, was capable of binding ispinesib, albeit at a significantly lower affinity than the nucleotide-bound form of the protein. Furthermore, these results showed that the ADP- and ATP$\gamma$S-bound forms of KSP had similar affinity for ispinesib. In the absence of $Mg^{2+}$ and at 0.5 mM ADP concentration, the KSP·ADP form showed 9.4 ± 0.2 °C $\Delta T_m$ in the presence of 50 $\mu$M ispinesib (Table 2). The $Mg^{2+}$-dependent difference in $\Delta T_m$ (~12.5 °C versus ~9.4 °C) for ispinesib binding to KSP·ADP was assumed to be the result of inefficient nucleotide binding in the absence of $Mg^{2+}$. TdCD results for monastrol binding to KSP·ADP and KSP alone were consistent with the ispinesib data (Figure 3, Tables 2 and 3). The KSP·ADP complex showed $\Delta T_m$ of 1.1 ± 0.14 °C in the presence of 50 $\mu$M monastrol corresponding to 10 $\mu$M TdCD $K_d$ at 20 °C. No significant $\Delta T_m$ shifts were seen for monastrol (Table 2), in the absence of nucleotide, implying poor affinity, at a level below the sensitivity limit for TdCD ($\Delta T_m$ < 0.5 °C).

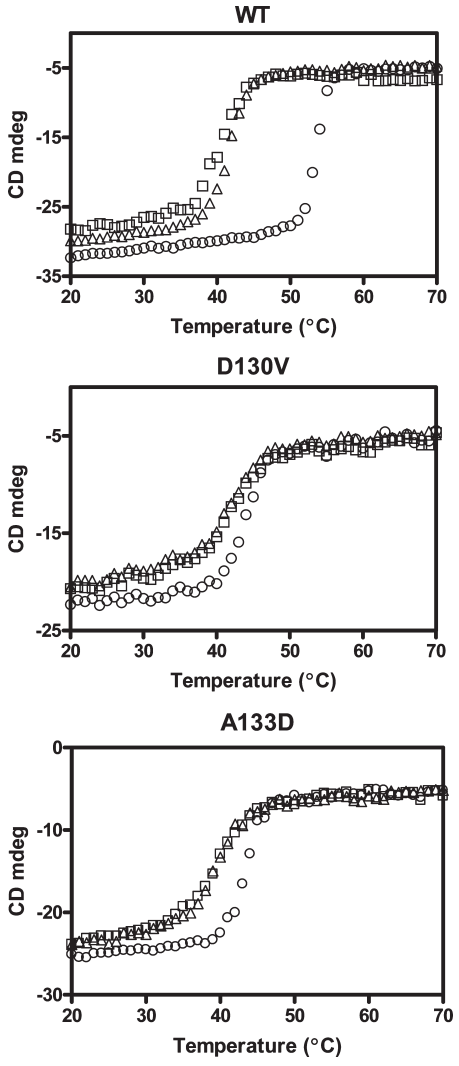


FIGURE 3: TdCD analyses of inhibitor binding to WT and mutant KSP forms. CD thermal denaturation curves for WT KSP (upper panel), D130V (middle panel), and A133D (lower panel) + ADP + $MgCl_2$ (□), + ADP + $MgCl_2$ + monastrol (△), and + ADP + $MgCl_2$ + ispinesib (○). Ellipticity (mdeg) was measured at 230 nm as a function of temperature (20−70 °C). Protein concentrations were 10−12 $\mu$M, ADP concentration was saturating at 0.25 mM, and inhibitor concentration was 50 $\mu$M in 20 mM PIPES, pH 7.5, 300 mM NaCl, 1 mM DTT, and 1% DMSO. The temperature was increased at 1 °C/min in a 1 mm path-length quartz cuvette.

*TdCD of Ispinesib-Resistant Mutants D130V and A133D: Nucleotide and Inhibitor Binding*. A133D KSP showed a weakly stabilizing shift in $T_m$ relative to the apo protein of approximately 1 ± 0.07 °C $\Delta T_m$ in the presence of 0.5 mM ATP$\gamma$S and 0.8 ± 0.07 °C $\Delta T_m$ in the presence of ADP (Table 5). This result suggested that the A133D mutant form bound nucleotides with lower affinity compared to its WT counterpart (2.4 ± 0.14 °C versus 1 ± 0.07 °C $\Delta T_m$ with 0.5 mM ATP$\gamma$S; Tables 2 and 5). Consistent with the A133D data, the TdCD experiments using D130V KSP demonstrated a significantly lower $\Delta T_m$ (< 0.5 °C) in the presence of 0.5 mM ATP$\gamma$S compared to WT KSP (Table 5). Thus, the TdCD analyses demonstrated that there was a significant difference in the nucleotide-binding affinity between WT and the D130V or A133D mutant KSP forms.

In the presence of 50 $\mu$M ispinesib, the A133D·ADP complex showed a $\Delta T_m$ of 3.9 ± 0.2 °C corresponding to 1 $\mu$M TdCD $K_d$ at 20 °C (Table 3). This TdCD result ($K_d$ at 20 °C) suggested that the A133D·ADP form bound ispinesib with ~1000-fold lower affinity than WT·ADP. For D130V·ADP, the $\Delta T_m$ for ispinesib, under similar experimental conditions, was 1.6 ± 0.09 °C (TdCD $K_d$ at 20 °C = 8 $\mu$M, Table 3), which is significantly lower than the WT as well as A133D form of the protein. More specifically, the binding affinity of ispinesib for D130V·ADP was 8000-fold and 8-fold lower compared to the affinity for WT·ADP and A133D·ADP, respectively. No significant $\Delta T_m$ shifts were seen for D130V·ADP and A133D·ADP in the presence of monastrol, implying that the affinity for monastrol was compromised and was below the limit of detection for TdCD ($\Delta T_m$ < 0.5 °C) and could not be assessed by this method.

*ITC of WT KSP: Binding of ADP, ATP$\gamma$S, Ispinesib, and Monastrol*. On the basis of the TdCD results, isothermal titration calorimetry (ITC) binding studies were performed to obtain a more complete thermodynamic analysis of nucleotide and inhibitor binding to KSP. Panels a and b of Figure 4 show

Table 3: TdCD Data for Binding of Ispinesib and Monastrol to WT, D130V, and A133D KSP

| | WT | | | D130V | | | A133D | | |
|---|---|---|---|---|---|---|---|---|---|
| preloaded mix (WT KSP + 0.25 mM ADP + 5 mM $MgCl_2$) | $T_m$ (°C) | $\Delta T_m$ (°C) | TdCD $K_d$[a] ($\mu$M) | $T_m$ (°C) | $\Delta T_m$ (°C) | TdCD $K_d$[a] ($\mu$M) | $T_m$ (°C) | $\Delta T_m$ (°C) | TdCD $K_d$[a] ($\mu$M) |
| +DMSO | 41.2 ± 0.07 | | | 42.2 ± 0.03 | | | 39.7 ± 0.06 | | |
| +50 $\mu$M ispinesib | 53.7 ± 0.2 | 12.5 ± 0.3 | 0.001 | 43.8 ± 0.06 | 1.6 ± 0.09 | 8 | 43.6 ± 0.17 | 3.9 ± 0.2 | 1 |
| +50 $\mu$M monastrol | 42.3 ± 0.07 | 1.1 ± 0.14 | 10 | 42.1 ± 0.1 | < 0.5 | > 30 | 39.7 ± 0.03 | < 0.5 | > 30 |

[a]Assuming $\Delta H_u$ = 100000 cal/mol and $\Delta H_L$ = −7000 cal/mol. Standard error values are from two to three experiments.

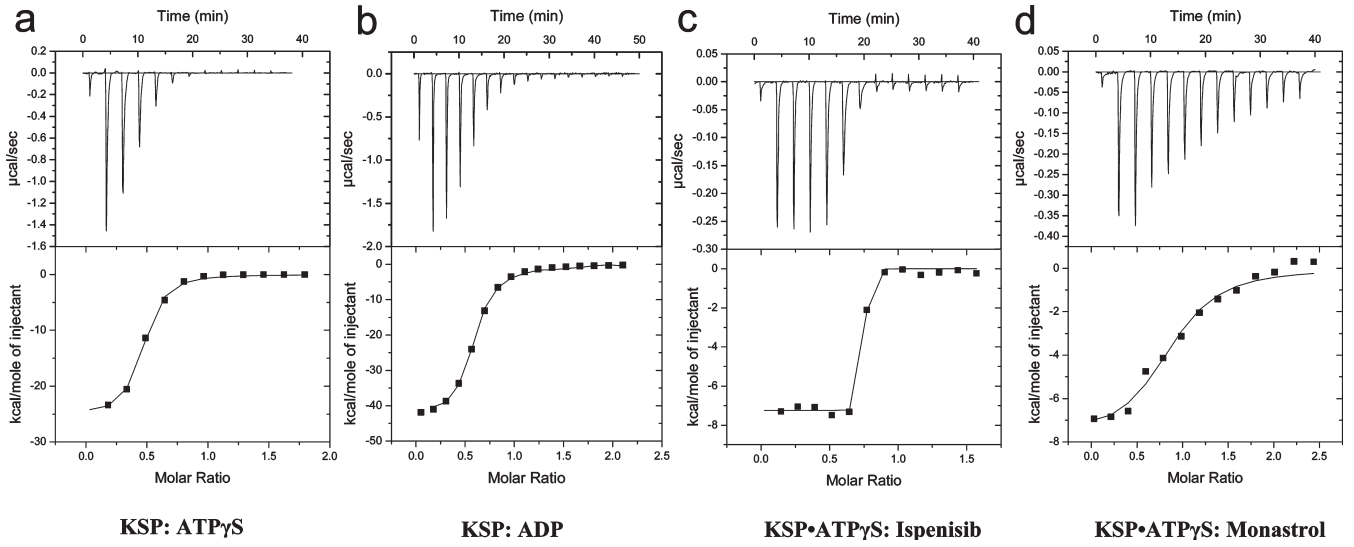


FIGURE 4: ITC analyses of nucleotide and inhibitor binding to WT KSP. Raw isothermal titration calorimetry data (upper panels) and normalized ITC data for titrations plotted versus the molar ratio of titrant/protein (lower panels) demonstrating saturable exothermic evolution of heat upon sequential additions of ATPγS (a) and ADP (b) to WT KSP in 20 mM PIPES, pH 7.5, 300 mM NaCl, 1 mM DTT, and 5 mM $MgCl_2$. (c) and (d) represent the raw ITC data (upper panels) and normalized ITC data for titrations plotted versus the molar ratio of titrant/protein (lower panels) for addition of ispinesib and monastrol, respectively, to WT KSP in 20 mM PIPES, pH 7.5, 300 mM NaCl, 1 mM DTT, 5 mM $MgCl_2$, and 0.5 mM ATPγS. Data analysis using Origin 5.0 software indicates that the binding data fit well to a single binding-site model.

Table 4: ITC Data for Binding of Nucleotides and Inhibitors to WT KSP

| preloaded mix (WT KSP) | ligand | ITC $K_d$[a] ($\mu$M) | $\Delta H$[a] (kcal/mol) | $T\Delta S$[a] (kcal/mol) |
|---|---|---|---|---|
| +5 mM $MgCl_2$ | ATPγS | 0.7 ± 0.04 | −25 ± 0.7 | −17 |
| +5 mM $MgCl_2$ | ADP | 0.6 ± 0.05 | −44 ± 2 | −35 |
| +500 $\mu$M ADP, 5 mM $MgCl_2$ | monastrol | 1.4 ± 0.1 | −8.5 ± 0.4 | −0.7 |
| +500 $\mu$M ATPγS, 5 mM $MgCl_2$ | monastrol | 2 ± 0.1 | −7.8 ± 0.4 | −0.2 |
| +500 $\mu$M ADP, 5 mM $MgCl_2$ | ispinesib | < 0.01 | −6.1 ± 0.2 | 5.2 |
| +500 $\mu$M ATPγS, 5 mM $MgCl_2$ | ispinesib | < 0.01 | −7.2 ± 0.1 | 5.1 |

[a]Determined at 293 K. $K_d$ values were calculated from ITC-derived $K_a$. Standard error values are from two to three experiments. The stoichiometry of complex formation was 0.85 ± 0.2. The low solubility of monastrol and ispinesib prevented accurate calorimetric determination of their binding thermodynamics in the absence of nucleotide.

representative calorimetric titration of KSP with ATPγS and ADP, respectively. The exothermic evolution of heat upon nucleotide injections shown in the upper panel illustrates saturable nucleotide binding by the protein. An analysis of the enthalpy change versus molar ratio of ATPγS/protein (lower panel) revealed an apparent $K_d$ for ATPγS of 0.7 ± 0.04 $\mu$M for KSP (Table 4). A similar experiment for ADP gave a $K_d$ of 0.6 ± 0.05 $\mu$M. Consistent with the TdCD $\Delta T_m$ results, WT KSP, in the absence of microtubules, bound ATPγS and ADP with comparable affinities. The $\Delta G$ for binding ADP was approximately −9 kcal/mol compared to a slightly lower −8 kcal/mol for ATPγS. A comparison of the $\Delta H$ and $T\Delta S$ shows that the binding interaction between KSP and nucleotide is predominantly enthalpic in nature. Interestingly, for WT KSP, the $\Delta H$ of binding for ADP was significantly more negative than that for ATPγS. The ITC-determined and TdCD-calculated $K_d$ for nucleotide binding to wild-type KSP were comparable when the ITC-measured $\Delta H_L$ value was considered for TdCD $K_d$ calculations. To determine if heats of protonation/ionization contribute to the observed $\Delta H$ of binding, the ITC experiment with ATPγS was repeated using HEPES buffer instead of PIPES. No significant difference in $K_d$, entropy, and enthalpy was observed (data not shown), indicating that the apparent $\Delta H$ values are similar to the intrinsic $\Delta H$ of binding and that the heat of protonation is not significant.

Figure 4c depicts ITC titration data of the KSP·ATPγS complex with ispinesib. The binding event is enthalpically ($\Delta H$ = −7.2 ± 0.1 kcal/mol) and entropically ($T\Delta S$ = 5.1 kcal/mol) favorable and has an ITC $K_d$ of < 0.01 $\mu$M (Table 4). Calorimetry of the KSP·ADP complex with ispinesib yielded similar affinity and relative enthalpic/entropic contributions (Table 4). The measured ITC and TdCD ITC $K_d$ for ispinesib binding to the KSP·ADP and KSP·ATPγS complex were thus quite consistent with each other. The representative titration of the KSP·ATPγS complex with monastrol is shown in Figure 4d. The $K_d$ of monastrol for KSP·ATPγS was 2 ± 0.1 $\mu$M. The binding of monastrol to the KSP·ATPγS complex was enthalpically driven ($\Delta H$ = −7.8 ± 0.4 kcal/mol) and entropically neutral ($T\Delta S$ = −0.2 kcal/mol). Similar results were obtained with the KSP·ADP complex (Table 4). Notably, the binding energy difference between monastrol and ispinesib is entropically dominated. The poor solubility of inhibitors prevented an accurate determination of their affinity to apo KSP (in the absence of nucleotides) by ITC. In the reverse titration (protein in syringe), KSP performed aberrantly and seemed to denature at low concentrations while stirring.

*ITC of KSP Mutants: Nucleotide Binding*. Table 5 summarizes the ITC-measured parameters for the binding of D130V and A133D mutants to ADP and ATPγS. For A133D, the ADP binding event is enthalpically favorable ($\Delta H$ = −27.5 ± 1.4 kcal/mol) and entropically unfavorable ($T\Delta S$ = −19.7 kcal/mol) and has an ITC $K_d$ of 3 ± 0.2 $\mu$M (Table 5). Compared to ADP, the ITC titration of A133D with ATPγS yielded ~3-fold lower $\Delta H$ and consequently a 2-fold higher ITC $K_d$. Thus, the A133D KSP mutant apo form showed significant ($p$ < 0.001) 5−10-fold higher ITC $K_d$ for nucleotide binding compared to its WT counterpart (Tables 4 and 5). Consistent with the TdCD results, D130V had the lowest affinity for nucleotides compared to WT and A133D KSP forms (Table 5). The binding of inhibitors to the mutants could not be assessed by ITC due to their limited solubilities and weak affinity.

*Modeling the Ispinesib Binding Mode*. The structure of the KSP·ADP·monastrol ternary complex offered the first view of an induced-fit pocket allosteric to the active site (*10*). The recently published crystal structure of a pyrrolotriazin-4-one (BMS-24) analogue of ispinesib bound to KSP·ADP (*27*) provided a compelling opportunity for modeling the binding interactions of ispinesib within the same binding site given the similarity between these two compounds. The docked model of ispinesib overlaid very closely atop BMS-24, with no significant conformational deviations (Figure 5 and see Supporting Information, Figure S3). Specifically, the quinazolinone occupies the hydrophobic groove flanked by L160, L214, G217, A218, and F239 as well as the salt bridge between E116 and R221. The carboxylate side chain of E116, as for BMS-24, serves as hydrogen bond acceptor for the aminopropyl moiety of ispinesib. The isopropyl substitution at the C-2 methyl of ispinesib remains in the same orientation as the cognate cyclopropyl of BMS-24, interacting with the side chain of Y211. The toluyl moiety makes hydrophobic contacts with the C$\beta$ atoms of D130V and A133. The conformations of the remaining ispinesib substitutents were indistinguishable from those of BMS-24, despite a lack of docking constraints. Finally, the ispinesib C-7 chlorine group is located in a small hydrophobic niche flanked by the aliphatic side chains of L214, A218, and L260 and the alkyl portion of the R221 side chain.

Table 5: TdCD and ITC Data for Binding of Nucleotides to A133D and D130V Mutant Forms of KSP

| KSP complex | ligand | $\Delta T_m$[a] (°C) | ITC $K_d$[b] ($\mu$M) | $\Delta H$[b] (kcal/mol) | $T\Delta S$[b] (kcal/mol) |
|---|---|---|---|---|---|
| A133D + 5 mM $MgCl_2$ | ATP$\gamma$S | 1 ± 0.07 | 7 ± 0.7 | −6.4 ± 0.3 | 0.47 |
| A133D + 5 mM $MgCl_2$ | ADP | 0.8 ± 0.07 | 3 ± 0.2 | −27.5 ± 1.4 | −19.7 |
| D130V + 5 mM $MgCl_2$ | ATP$\gamma$S | < 0.5 | | −3.2 ± 0.6 | |
| D130V + 5 mM $MgCl_2$ | ADP | < 0.5 | 6 ± 0.3 | −10.2 ± 1 | −3 |

[a]Determined at 500 $\mu$M nucleotide concentration. [b]Determined at 293 K. $K_d$ values were calculated from ITC-derived $K_a$. Standard error values are from two to three experiments. The stoichiometry of complex formation was 0.9 ± 0.2. The low $\Delta H$ of ATP$\gamma$S for D130V prevented accurate calorimetric determination of the binding $K_d$ in $ITC_{200}$.

## DISCUSSION

An induced-fit pocket formed by helices α2 and α3 and loop L5 has been identified as an allosteric site for inhibiting the ATPase activity of the motor domain of the mitotic kinesin KSP (Eg5) (*10*). Although many potent and distinct chemotypes are known, monastrol and the quinazolinone analogues represented by ispinesib have been the most thoroughly characterized in both the scientific and patent literature. More importantly, ispinesib resistance mutations were recently observed and could be localized to D130V and A133D in the L5 loop (*16*, *21*). The colon carcinoma cell line HFT116 harboring these mutations was ca. 100-fold less susceptible to the antiproliferative effect of ispinesib (*16*). The effect of mutagenesis in the induced-fit pocket and the binding modes of corresponding inhibitors determined by X-ray crystallography, together with the thermodynamic data presented here, provide a unique opportunity to map further that site and guide future structure-based design activities.

Our enzyme kinetic studies of the purified forms of wild-type, D130V, and A133D KSP indicated that the mutations resulted in a modest decrease in the ATPase catalytic efficiency. The D130V mutation had a more pronounced effect than A133D, i.e., a 3-fold versus 2-fold decrease in catalytic efficiency (Table 1). In contrast to the effect on catalytic efficiency, the effect on ispinesib and monastrol inhibition of ATPase activities was much more dramatic. For ispinesib, the increase in IC50 was between 2 and 3 orders of magnitude for the two mutants versus wild type. Interestingly, the pattern of increase in IC50 from wild type to mutants mirrors the effect on catalytic efficiency. Based on enzymatic activity, D130V was more resistant than A133D to ispinesib.

Using both thermal denaturation and calorimetric techniques to assess ligand binding, we confirm the essential role of ATP$\gamma$S/$Mg^{2+}$ or ADP/$Mg^{2+}$ in forming the optimum KSP conformation for binding inhibitors, in other words, the optimum conformation of the induced-fit binding pocket. The thermal stability of the wild-type motor domain increased by 2−2.5 °C in the presence of either 0.5 mM ATP$\gamma$S or ADP and 5 mM $MgCl_2$, which translates into a submicromolar calculated $K_{d20°C}$ by substituting the measured $\Delta H_L$ of 20−40 kcal/mol (Table 2). The binding constant derived from ITC and thermal denaturation studies (calculated based on measured $\Delta H$) was markedly different from

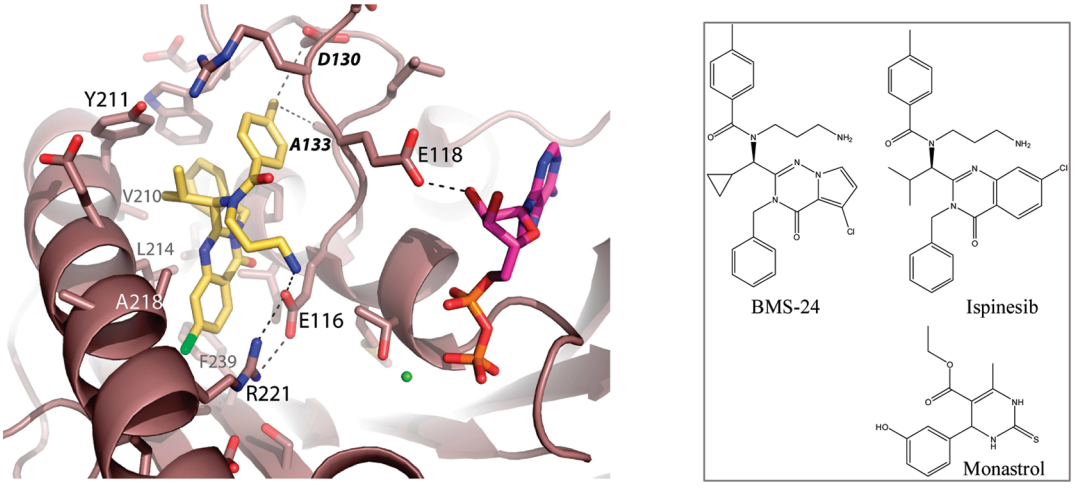


FIGURE 5: Mode of ispinesib binding to KSP. The left panel depicts the docked conformation of ispinesib (yellow carbon atoms) in complex with KSP·ADP/$Mg^{2+}$. KSP side-chain atoms within 5 Å of ispinesib are shown explicitly in stick representation. The right panel shows two-dimensional depictions of BMS-24, ispinesib, and monastrol.

the $K_m$ value for ATP obtained from steady-state kinetic analysis ($K_m$ = 38 $\mu$M versus $K_{d20°C}$ = 0.7 $\mu$M (ATP$\gamma$S)). The presence of microtubule in the enzyme assay mixture seems to have a significant effect on the affinity of ATP for the KSP motor domain. Interestingly, the ITC measured $K_d$ for ADP binding to apo KSP is within 2-fold of the published $K_i$ values (1.5 $\mu$M) for ADP in basal ATPase assay (*33*). In the same study, the authors showed the $K_i$ value for ADP in MT-stimulated KSP ATPase activity assay was 92 $\mu$M (compared to 1.5 $\mu$M in the absence of MT), implying the presence of microtubules could indeed impact the affinity of the nucleotides.

High-affinity binding of inhibitors, either monastrol or ispinesib, is highly dependent on preincubation of the motor domain with the nucleotide/$Mg^{2+}$ complex. For example, in the absence of ADP, ispinesib binds at low affinity (TdCD $K_{d20°C}$ = 3 $\mu$M), and upon preincubation with both ADP and $Mg^{2+}$, its affinity increases by 3000-fold (TdCD $K_{d20°C}$ = 1 nM) (Table 3). A similar effect was found for monastrol; in the absence of ADP, its binding to KSP could not be demonstrated using TdCD within the limit of detection ($\Delta T_m$ < 0.5 °C). However, in the presence of ADP/$Mg^{2+}$, a calculated TdCD $K_{d20°C}$ of 10 $\mu$M for monastrol binding could clearly be distinguished. Our results are consistent with the induced-fit binding site originally described for monastrol (*10*). It is also clear that these inhibitors prefer the nucleotide-bound forms of the enzyme. Nucleotide-mediated improvement in inhibitor binding affinity could be explained by nucleotide-induced ordering of the L5 loop via interaction with E118 (Figure 5). Kinetic evidence provided by others appears to indicate that the mechanism of inhibition consists of slowing the rate of ADP release and decreasing the KSP microtubule affinity (*11*). All data also imply that ATP/$Mg^{2+}$ or ADP/$Mg^{2+}$ induces a structural conformation distinct from the apo form of KSP prior to inhibitor docking onto the induced-fit binding site. An X-ray structure of apo KSP has yet to be reported for comparison with the available structure of KSP·ADP/$Mg^{2+}$ (*32*).

Isothermal titration calorimetric studies provide additional information about the binding energetics of the nucleotide/$Mg^{2+}$ complexes and inhibitors to both wild-type KSP and mutants. Notably, the free energy of nucleotide binding was enthalpically driven and entropically unfavorable (Table 4). This entropic penalty is consistent with the conformational restrictions of the nucleotide in the polar environment near the N-terminus of helix α2 and the P-loop, which accommodates the α- and $\beta$-phosphates of ADP. Two hydrogen bonds are observed between the ADP 2′OH and the carboxylate side chain of E118 and between O3 of the α-phosphate and backbone amide of G110 (*32*).

The binding energetics of monastrol in the presence of ADP/$Mg^{2+}$ was also essentially enthalpic ($\Delta H \sim -8$ kcal/mol) with a rather small entropic contribution. Although it is difficult to pinpoint the exact structural basis of the negative enthalpy, the hydrogen bonds observed between monastrol and KSP·ADP/$Mg^{2+}$ (N-1-pyrimidine to backbone carbonyl of E116; phenolic OH to backbone carbonyl of E118) could certainly play a significant role. In addition, accommodation of monastrol into the induced-fit pocket results in an inward relocation of the W127 side chain (loop L5) for face-to-edge interaction with the monastrol phenolic moiety and outward flipping of R119 (of helix α2) and Y211 (of helix α3) toward the bulk solvent. The net effect dominated by enhanced solvation of the guanidinium and phenolic OH of R119 and Y211, respectively, could further contribute to the enthalpy observed in ITC.

In contrast to monastrol, the high-affinity binding of ispinesib was the consequence of both favorable enthalpy ($\Delta H \sim -7$ kcal/mol) and entropy ($T\Delta S \sim 5$ kcal/mol). The result could be further validated by inspecting the model of ispinesib bound to the induced-fit pocket (Figure 5 and Supporting Information, Figure S3). Ispinesib forms a single hydrogen bond with KSP·ADP/$Mg^{2+}$ (aminopropyl to carboxylate side chain of E116) compared to two hydrogen bond interactions for monastrol. All other interactions are predominantly hydrophobic in nature, especially in regard to accommodation of the pyrrole ring (L160, I136, L214, and F239) with the 6-chloro pointing directly toward F239 and I136; N-3 benzyl (face-to-edge interaction with W127 and flanking by P139); C-2-methyl-isopropyl (packing against the aromatic side chain of Y211). The contribution of the face-to-edge interaction between ispinesib N-3-benzyl and 4-methylbenzamide to binding entropy remains to be determined since it could still be a preexisting intrinsic conformation of the compound in solution before docking into the induced-fit pocket.

The effect of D130V or A133D mutations on the binding affinity of ispinesib and monastrol has its basis in the integrity of the binding pocket accommodating the 4-methylbenzamide and phenolic moieties, respectively. It happens to be near the base of the L5 loop, which is known to undergo major conformation rearrangement upon inhibitor docking (*10*). Both residues, D130 and A133, are engaged in an extensive hydrogen bond network between each other and with neighboring residues. More specifically, the backbone amide nitrogen of A133 is hydrogen bonded to the backbone carbonyl of D130, which is in turn hydrogen bonded to the backbone amide nitrogen of L132. The backbone amide nitrogen of D130, on the other hand, hydrogen bonds to the carbonyl of T126, helping to maintain loop L5 in the inward conformation essential for inhibitor binding. Finally, the carboxylate side chain of D130 extends the network by reaching out to neighboring S120 (side chain OH), R119 (guanidinium Nε), and L132 (backbone NH). The hydrogen bond network extending from D130 and A133 seems to hold the key to the architecture required for high-affinity inhibitor binding. By association, neighboring residues in hydrogen bond interactions with D130 and A133 are most likely sensitive sites for resistance mutations.

Interestingly, the enzymatic data showed differences in the $K_{mATP}$ for WT and ispinesib-resistant mutants (Table 1). Direct binding experiments using TdCD and ITC corroborated the enzymatic assay results (Tables 4 and 5). While the wild-type enzyme bound nucleotides with submicromolar affinity, the mutant counterparts showed 6−10-fold higher ITC $K_d$ for the nucleotides. The differences in the ITC $K_d$ appeared to be the direct consequence of a lower enthalpy of nucleotide binding in the mutants compared to the WT KSP. Notably, the nucleotide binding affinity for KSP proteins had the rank order WT > A133D > D130V consistent with the measured enzymatic $K_{mATP}$. These data indicate potential allosteric structural rearrangement in the nucleotide binding site as a consequence of mutations in the neighboring induced-fit binding pocket.

## CONCLUSION

Site-directed mutagenesis has always been a tool of choice for probing the architecture of enzyme inhibitor binding sites, especially for enzyme targets that are of high therapeutic value. When used in conjunction with biophysical tools such as thermal denaturation, isothermal calorimetry, and available X-ray crystal structures, the quality of mapping of the binding is much enhanced. Our studies of the KSP motor domain, together with

two allosteric inhibitors, monastrol and ispinesib, and two resistance mutants provide a detailed view of a well-established induced-fit inhibitor binding site, both in thermodynamic and in structural terms. The studies point to a subdomain within the pocket that could be highly sensitive to resistance mutations. Furthermore, the results serve as future guidance for design of better inhibitors as candidates for selective antimitotic anticancer drug development.

## ACKNOWLEDGMENT

We thank Dr. Charles McNemar and Dr. Cheng-Chi Chuang for performing N-terminal sequencing and mass spectrometry, respectively, and Dr. William Windsor for critical reading of the manuscript.

## SUPPORTING INFORMATION AVAILABLE

The kinetic and thermodynamic parameters measured for the KSP proteins (Table S1), purity and solution behavior of the three purified KSP proteins used for kinetic and thermodynamic characterization (Figures S1 and S2), and stereo illustration of the docked conformation of ispinesib in complex with KSP·ADP/$Mg^{2+}$ (Figure S3). This material is available free of charge via the Internet at http://pubs.acs.org.

## REFERENCES

1. Miki, H., Okada, Y., and Hirokawa, N. (2005) Analysis of the kinesin superfamily: Insights into structure and function. *Trends Cell Biol. 15*, 467–476.
2. Kapitein, L. C., Peterman, E. J. G., Kwok, B. H., Kim, J. H., Kapoor, T. M., and Schmidt, C. F. (2005) The bipolar mitotic kinesin Eg5 moves on both microtubules that it crosslinks. *Nature 435*, 114–118.
3. Kashina, A. S., Rogers, G. C., and Scholey, J. M. (1997) The bimC family of kinesins: Essential bipolar mitotic motors driving centrosome separation. *Biochim. Biophys. Acta 1357*, 257.
4. Sharp, D. J., Rogers, G. C., and Scholey, J. M. (2000) Microtubule motors in mitosis. *Nature 407*, 41–47.
5. Guellec, R. L., Paris, J., Couturier, A., Roghi, C., and Philippe, M. (1991) Cloning by differential screening of a *Xenopus* cDNA that encodes a kinesin-related protein. *Mol. Cell. Biol. 11*, 3395–3398.
6. Jackson, J. R., Patrick, D. R., Dar, M. M., and Huang, P. S. (2007) Targeted anti-mitotic therapies: Can we improve on tubulin agents? *Nat. Rev. Cancer 7*, 107–117.
7. Mayer, T. U., Kapoor, T. M., Haggarty, S. J., King, R. W., Schreiber, S. L., and Mitchison, T. J. (1999) Small molecule inhibitor of mitotic spindle bipolarity identified in a phenotype-based screen. *Science 286*, 971–974.
8. DeBonis, S., Simorre, J.-P., Crevel, I., Lebeau, L., Skoufias, D. A., Blangy, A., Ebel, C., Gans, P., Cross, R., Hackney, D. D., Wade, R. H., and Kozielski, F. (2003) Interaction of the mitotic inhibitor monastrol with human kinesin Eg5. *Biochemistry 42*, 338–349.
9. Maliga, Z., Kapoor, T. M., and Mitchison, T. J. (2002) Evidence that monastrol is an allosteric inhibitor of the mitotic kinesin Eg5. *Chem. Biol. 9*, 989–996.
10. Yan, Y., Sardana, V., Xu, B., Homnick, C., Halczenko, W., Buser, C. A., Schaber, M., Hartman, G. D., Huber, H. E., and Kuo, L. C. (2004) Inhibition of a mitotic motor protein: Where, how and conformational consequences. *J. Mol. Biol. 335*, 547–554.
11. Lad, L., Luo, L., Carson, J. D., Wood, K. W., Hartman, J. J., Copeland, R. A., and Sakowicz, R. (2008) Mechanism of inhibition of human KSP by ispinesib. *Biochemistry 47*, 3576−3585.
12. Cox, C. D., Coleman, P. J., Breslin, M. J., Whitman, D. B., Garbaccio, R. M., Fraley, M. E., Buser, C. A., Walsh, E. S., Schaber, M. D., Lobell, R. B., Tao, W., Davide, J. P., Diehl, R. E., Abrams, M. T., South, V. J., Huber, H. E., Torrent, M., Prueksaritanont, T., Li, C., Slaughter, D. E., Mahan, E., Fernandez-Metzler, C., Yan, Y., Kuo, L. C., Kohl, N. E., and Hartman, G. D. (2008) Kinesin spindle protein (KSP) inhibitors. 9. Discovery of (2*S*)-4-(2,5-difluorophenyl)-*N*-[(3*R*,4*S*)-3-fluoro-1-methylpiperidin-4-yl]-2-(hydroxymethyl)-*N*-methyl-2-phenyl-2,5-dihydro-1*H*-pyrrole-1-carboxamide (MK-0731) for the treatment of taxane-refractory cancer. *J. Med. Chem. 51*, 4239–4252.
13. Cox, C. D., Breslin, M. J., Mariano, B. J., Coleman, P. J., Buser, C. A., Walsh, E. S., Hamilton, K., Huber, H. E., Kohl, N. E., Torrent, M., Yan, Y., Kuo, L. C., and Hartman, G. D. (2005) Kinesin spindle protein (KSP) inhibitors. Part 1: The discovery of 3,5-diaryl-4,5-dihydropyrazoles as potent and selective inhibitors of the mitotic kinesin KSP. *Bioorg. Med. Chem. Lett. 15*, 2041–2045.
14. Cox, C. D., Torrent, M., Breslin, M. J., Mariano, B. J., Whitman, D. B., Coleman, P. J., Buser, C. A., Walsh, E. S., Hamilton, K., Schaber, M., Lobell, R. B., Tao, W., South, V. J., Kohl, N. E., Yan, Y., Kuo, L. C., Prueksaritanont, T., Slaughter, D. E., Li, C., Mahan, E., Lu, B., and Hartman, G. D. (2006) Kinesin spindle protein (KSP) inhibitors. Part 4: Structure-based design of 5-alkylamino-3,5-diaryl-4,5-dihydropyrazoles as potent and water soluble inhibitors of the mitotic kinesin KSP. *Bioorg. Med. Chem. Lett. 16*, 3175–3179.
15. DeBonis, S., Skoufias, D. A., Indorato, R.-L., Liger, F., Marquet, B., Laggner, C., Benoit, J., and Kozielski, F. (2008) Structure −activity relationship of *S*-trityl-L-cysteine analogues as inhibitors of the human mitotic kinesin Eg5. *J. Med. Chem. 51*, 1115–1125.
16. Luo, L., Parrish, C. A., Neysa, N., McNulty, D. E., Chaudhari, A. M., Carson, J. D., Sudakin, V., Shaw, A. N., Lehr, R., Zhao, H., Sweitzer, S., Lad, L., Wood, K. W., Sakowicz, R., Annan, R. S., Huang, P. S., Jackson, J. R., Dhanak, D., Copeland, R. A., and Auger, K. R. (2007) ATP-competitive inhibitors of the mitotic kinesin KSP that function via an allosteric mechanism. *Nat. Chem. Biol. 3*, 722–726.
17. Rickert, K. W., Schaber, M., Torrent, M., Neilson, L. A., Tasber, E. S., Garbaccio, R., Coleman, P. J., Harvey, D., Zhang, Y., Yang, Y., Marshall, G., Lee, L., Walsh, E. S., Hamilton, K., and Buser, C. A. (2008) Discovery and biochemical characterization of selective ATP competitive inhibitors of the human mitotic kinesin KSP. *Arch. Biochem. Biophys. 469*, 220–231.
18. Cochran, J. C., and Gilbert, S. P. (2005) ATPase mechanism of Eg5 in the absence of microtubules: Insights into microtubule activation and allosteric inhibition by monastrol. *Biochemistry 44*, 16633–16648.
19. Cochran, J. C., Gatial, J. E., III, Kapoor, T. M., and Gilbert, S. (2005) Monastrol inhibition of the mitotic kinesin Eg5. *J. Biol. Chem. 280*, 12658–12667.
20. Lad, L., Luo, L., Carson, J. D., Wood, K. W., Hartman, J. J., Copeland, R. A., and Sakowicz, R. (2008) Mechanism of inhibition of human KSP by ispinesib. *Biochemistry 47*, 3576–3585.
21. Jackson, J. R., Auger, K. R., Gilmartin, A., Wai, E. K., Luo, L., Concha, N., Parrish, C. A., Sutton, D., Diamond, M. A., Giardiniere, M., Zhang, S.-Y., Huang, P. S., Wood, K. W., Belmont, L., Lee, Y., Bergnes, G., Anderson, R., Brejc, K., Sakowicz, R. (2005) A resistance mechanism for the KSP inhibitor ispinesib implicates point mutations in the compound binding site, in Proceedings of the AACR-NCI-EORTC Molecular Targets and Cancer Therapeutics Meeting, AACR, Philadelphia, PA.
22. Yang, J., Wu, C., and Martinez, H. (1986) Calculation of protein conformation from circular dichroism. *Methods Enzymol. 130*, 208–269.
23. Waldron, T. T., and Murphy, K. P. (2003) Stabilization of proteins by ligand binding: Application to drug screening and determination of unfolding energetics. *Biochemistry 42*, 5058–5064.
24. Brandts, J. F., and Lin, L. N. (1990) Study of strong ultratight protein interactions using differential scanning calorimetry. *Biochemistry 29*, 6927–6940.
25. Mayhood, T. W., and Windsor, W. T. (2005) Ligand binding affinity determined by temperature-dependent circular dichroism: Cyclin-dependent kinase 2 inhibitors. *Anal. Biochem. 345*, 187–197.
26. Pantoliano, M. L., Petrella, E. C., Kwasnoski, J. D., Lobanov, V. S., Myslik, J., Graf, E., Carver, T., Asel, E., Springer, B. A., Lane, P., and Salemme, F. R. (2001) High-density miniaturized thermal shift assays as a general strategy for drug discovery. *J. Biomol. Screen. 6*, 429–440.
27. Kim, K. S., Lu, S., Cornelius, L. A., Lombardo, L. J., Borzilleri, R. M., Schroeder, G. M., Sheng, C., Rovnyak, G., Crews, D., Schmidt, R. J., Williams, D. K., Bhide, R. S., Traeger, S. C., McConnell, P. A., Mueller, L., Sheriff, S., Newitt, J. A., Pudzianowski, A., Yang, Z., Wild, R., Lee, F. Y., Batorsky, R., Ryder, J. S., Ortega-Nanos, M., Shen, H., Gottardis, M., and Roussell, D. L. (2006) Synthesis and SAR of pyrrolotriazine-4-one based Eg5 inhibitors. *Bioorg. Med. Chem. Lett. 16*, 3937–3942.
28. Schrödinger, L., New York, NY (2007).
29. Friesner, R. A., Banks, J. L., Murphy, R. B., Halgren, T. A., Klicic, J. J., Mainz, D. T., Repasky, M. P., Knoll, E. H., Shelley, M., Perry, J. K., Shaw, D. E., Francis, P., and Shenkin, P. S. (2004) Glide: A new approach for rapid, accurate docking and scoring. 1. Method and assessment of docking accuracy. *J. Med. Chem. 47*, 1739–1749.
30. Halgren, T. A., Murphy, R. B., Friesner, R. A., Beard, H. S., Frye, L. L., Pollard, T. W., and Banks, J. L. (2004) Glide: A new approach for

rapid, accurate docking and scoring. 2. Enrichment factors in database screening. *J. Med. Chem. 47*, 1750–1759.
31. Luo, L., Carson, J. D., Dhanak, D., Jackson, J. R., Huang, P. S., Lee, Y., Sakowicz, R., and Copeland, R. A. (2004) Mechanism of inhibition of human KSP by monastrol: Insights from kinetic analysis and the effect of ion strength on KSP inhibition. *Biochemistry 43*, 15258–15266.
32. Turner, J., Anderson, R., Guo, J., Beraud, C., Fletterick, R., and Sakowicz, R. (2001) Crystal structure of the mitotic spindle kinesin Eg5 reveals a novel conformation of the neck-linker. *J. Biol. Chem. 276*, 25496–25502.
33. Luo, L., Carson, J. D., Molnar, K. S., Tuske, S. J., Coales, S. J., Hamuro, Y., Sung, C.-m., Sudakin, V., Auger, K. R., Dhanak, D., Jackson, J. R., Huang, P. S., Tummino, P. J., and Copeland, R. A. (2008) Conformation-dependent ligand regulation of ATP hydrolysis by human KSP: Activation of basal hydrolysis and inhibition of microtubule-stimulated hydrolysis by a single, small molecule modulator. *J. Am. Chem. Soc. 130*, 7584–7591.